AIP Conference Proceedings

A real two-phase submarine debris flow and tsunami

Shiva P. Pudasaini and Stephen A. Miller

Citation: AIP Conf. Proc. **1479**, 197 (2012); doi: 10.1063/1.4756096
View online: http://dx.doi.org/10.1063/1.4756096
View Table of Contents: http://proceedings.aip.org/dbt/dbt.jsp?KEY=APCPCS&Volume=1479&Issue=1
Published by the American Institute of Physics.

A Real Two-Phase Submarine Debris Flow and Tsunami

Shiva P. Pudasaini and Stephen A. Miller

Department of Geodynamics and Geophysics, Steinmann Institute, University of Bonn
Nussallee 8, D-53115, Bonn, Germany

Abstract. The general two-phase debris flow model proposed by Pudasaini [1] is employed to study subaerial and submarine debris flows, and the tsunami generated by the debris impact at lakes and oceans. The model, which includes three fundamentally new and dominant physical aspects such as enhanced viscous stress, virtual mass, and generalized drag (in addition to buoyancy), constitutes the most generalized two-phase flow model to date. The advantage of this two-phase debris flow model over classical single-phase, or quasi-two-phase models, is that the initial mass can be divided into several parts by appropriately considering the solid volume fraction. These parts include a dry (landslide or rock slide), a fluid (water or muddy water; e.g., dams, rivers), and a general debris mixture material as needed in real flow simulations. This innovative formulation provides an opportunity, within a single framework, to simultaneously simulate the sliding debris (or landslide), the water lake or ocean, the debris impact at the lake or ocean, the tsunami generation and propagation, the mixing and separation between the solid and fluid phases, and the sediment transport and deposition process in the bathymetric surface. Applications of this model include (*a*) sediment transport on hill slopes, river streams, hydraulic channels (e.g., hydropower dams and plants); lakes, fjords, coastal lines, and aquatic ecology; and (*b*) submarine debris impact and the rupture of fiber optic, submarine cables and pipelines along the ocean floor, and damage to offshore drilling platforms. Numerical simulations reveal that the dynamics of debris impact induced tsunamis in mountain lakes or oceans are fundamentally different than the tsunami generated by pure rock avalanches and landslides. The analysis includes the generation, amplification and propagation of super tsunami waves and run-ups along coastlines, debris slide and deposition at the bottom floor, and debris shock waves. It is observed that the submarine debris speed can be faster than the tsunami speed. This information can be useful for early warning strategies in the coastal regions. These findings substantially increase our understanding of complex multi-phase systems and multi-physics and flows, and allows for the proper modeling of landslide and debris induced tsunami, the dynamics of turbidity currents and sediment transport, and the associated applications to hazard mitigation, geomorphology and sedimentology.

Keywords: Non-Newtonian Multiphase Flows, Submarine Landslides, Sediment Transport, Turbidity Current, Tsunamis, Hydropower Dams
PACS: 45.70.Ht, 47.35.Bb, 47.50.-d, 47.55.-t, 88.60.jb, 91.30.Nw, 91.50.Xz, *91.62.Ty, 92.10.Wa, *92.10.hl, 92.40.Gc, 92.40.Ha

INTRODUCTION

Debris flows and induced super tsunamis are extremely destructive and dangerous natural hazards [2,3] so there is a need for reliable methods for predicting the dynamics, the runout distances, and the inundation areas of such events. Debris flows are multiphase, gravity-driven flows consisting of a broad distribution of grain sizes mixed with fluid. The rheology and flow behavior varies depending on the sediment composition and the percentage of solid and fluid phases. Research in previous decades focused on different aspects of single- and two-phase debris avalanches and debris flows and induced tsunami [2-11], which was recently advanced by Pudasaini [1] with a comprehensive theory that accounts for interactions between the solid and the fluid . The model, which includes buoyancy, also includes three new and important dominant physical aspects of solid-volume-fraction-gradient-enhanced non-Newtonian viscous stress, virtual mass, and generalized drag. This model constitutes the most generalized two-phase flow model to date, and can reproduce results from most previous simple models that considered single- and two-phase avalanches and debris flows as special cases [4,5,7,8].

To develop insight into the basic features of the complex non-linear equations, the model is applied to simple, one-dimensional debris flow and tsunami generation. Here, we focus primarily on the complex dynamics of a two-phase subaerial debris flow sliding down an inclined channel plunging into a fluid dam. The impact produces a tsunami wave while at the same time generates a submarine debris flow along the dam basin. Simulation results show that the amount of grain in the dam plays a significant role in controlling the overall dynamics of the tsunami wave and the submarine debris flow. For very small solid particle concentrations in the dam, the submarine debris flow moves significantly faster than the surface tsunami wave, which may be an observable phenomena in nature. We also investigated the complex interactions between the submarine debris wave and the tsunami wave, which to date have not been available. These results demonstrate wide applicability of the model to a wide range of two-phase geophysical mass flows,

Numerical Analysis and Applied Mathematics ICNAAM 2012
AIP Conf. Proc. 1479, 197-200 (2012); doi: 10.1063/1.4756096

including particle-laden and dispersive flows, sediment transport, and debris flows.

DESCRIPTION OF A GENERAL TWO-PHASE DEBRIS FLOW MODEL

We consider the general two-phase debris flow model [1] reduced to one-dimensional channel flows. The depth-averaged mass and momentum conservation equations for the solid and fluid phases are:

$$\frac{\partial}{\partial t}(\alpha_s h)+\frac{\partial}{\partial x}(\alpha_s h u_s)=0,\;\; \frac{\partial}{\partial t}(\alpha_f h)+\frac{\partial}{\partial x}(\alpha_f h u_f)=0, \tag{1}$$

$$\frac{\partial}{\partial t}\left[\alpha_s h\left(u_s-\gamma\, C\left(u_f-u_s\right)\right)\right]+\frac{\partial}{\partial x}\left[\alpha_s h\left(u_s^2-\gamma\, C\left(u_f^2-u_s^2\right)+\beta_s\frac{h}{2}\right)\right]=hS_s, \tag{2}$$

$$\frac{\partial}{\partial t}\left[\alpha_f h\left(u_f+\frac{\alpha_s}{\alpha_f}C\left(u_f-u_s\right)\right)\right]+\frac{\partial}{\partial x}\left[\alpha_f h\left(u_f^2+\frac{\alpha_s}{\alpha_f}C\left(u_f^2-u_s^2\right)+\beta_f\frac{h}{2}\right)\right]=hS_f, \tag{3}$$

in which $\beta_s=\varepsilon K p_{b_s}$, $\beta_f=\varepsilon p_{b_f}$, $p_{b_f}=-g^z$, $p_{b_s}=(1-\gamma)p_{b_f}$. In (2)-(3) the source terms are

$$S_s=\alpha_s\left[g^x-\frac{u_s}{|u_s|}\tan\delta p_{b_s}-\varepsilon p_{b_s}\frac{\partial b}{\partial x}\right]-\varepsilon\alpha_s\gamma p_{b_f}\left[\frac{\partial h}{\partial x}+\frac{\partial b}{\partial x}\right]+C_{DG}\left(u_f-u_s\right)|u_f-u_s|^{J-1}, \tag{4}$$

$$\begin{aligned}S_f=\alpha_f&\left[g^x-\varepsilon\left[\frac{1}{2}p_{b_f}\frac{h}{\alpha_f}\frac{\partial\alpha_s}{\partial x}+p_{b_f}\frac{\partial b}{\partial x}-\frac{1}{\alpha_f N_R}\left\{2\frac{\partial^2 u_f}{\partial x^2}-\frac{\chi u_f}{\varepsilon^2h^2}\right\}\right.\right.\\ &\left.\left.+\frac{1}{\alpha_f N_{R_A}}\left\{2\frac{\partial}{\partial x}\left(\frac{\partial\alpha_s}{\partial x}\left(u_f-u_s\right)\right)\right\}-\frac{\xi\alpha_s\left(u_f-u_s\right)}{\varepsilon^2\alpha_f N_{R_A}h^2}\right]\right]-\frac{1}{\gamma}C_{DG}\left(u_f-u_s\right)|u_f-u_s|^{J-1},\end{aligned} \tag{5}$$

where

$$\begin{aligned}&C_{DG}=\frac{\alpha_s\alpha_f(1-\gamma)}{\left[\varepsilon U_T\{PF(Re_p)+(1-P)G(Re_p)\}\right]^J},\;\; F=\frac{\gamma}{180}\left(\alpha_f/\alpha_s\right)^3Re_p,\;\; G=\alpha_f^{M(Re_p)-1},\\ &\gamma=\frac{\rho_f}{\rho_s},\; C=\frac{1}{2}\left(\frac{1+2\alpha_s}{\alpha_f}\right),\; Re_p=\frac{\rho_f d\; U_T}{\eta_f},\; N_R=\frac{\sqrt{gL}H\rho_f}{\alpha_f\eta_f}, N_{R_A}=\frac{\sqrt{gL}H\rho_f}{A\eta_f}.\end{aligned} \tag{6}$$

where x and z are coordinates along the flow directions, and g^x and g^z are the components of gravitational acceleration. The solid and fluid constituents are denoted by s and f, h is the flow depth, and u_s and u_f are the solid and fluid velocities. ρ_s, ρ_f, and α_s, α_f denote the densities and volume fractions of the solid and the fluid, respectively. L and H are the typical length and depth of the flow, $\varepsilon=H/L$ is the aspect ratio, and $\mu=\tan\delta$ is the basal friction coefficient. K is the earth pressure coefficient (function of δ, and ϕ, basal and internal friction angles of solid), C_{DG} is the generalized drag coefficient, $J=1$ or 2 represents linear or quadratic drag. U_T is the terminal velocity of a particle and $P\in[0,1]$ is a parameter which combines the solid-like (G) and fluid-like (F) drag contributions to flow resistance. p_{b_f} and p_{b_s} are the effective fluid and solid pressures. γ is the density ratio, C is the virtual mass coefficient (solid particles induced kinetic energy of fluid phase), η_f is the fluid viscosity, M is a function of the particle Reynolds number (Re_p), χ includes vertical shearing of fluid velocity, and ξ takes into account different distributions of α_s. $A=A(\alpha_f)$ is the mobility of the fluid at the interface, and N_R and N_{R_A} are Reynolds numbers associated with the classical Newtonian, and enhanced non-Newtonian fluid viscous stresses. Slope topography is represented by $b=b(x)$. Coulomb and no-slip boundary conditions are employed for the solid and the fluid.

There are two important aspects of the model equations. First, the inertial terms on the left hand side of (2)-(3) includes the lateral pressure (associated with β_s and β_f) and the virtual mass, C. Secondly, the source in the solid momentum (4) has three different contributions from (*i*) gravity, the Coulomb friction and the slope gradient (first square bracket); (*ii*) terms associated with the buoyancy force (second square bracket); and (*iii*) the generalized drag contribution (C_{DG}) (last term). The source term for the fluid momentum equation, (5) has six different contributions; the first three terms emerge from the gravity load (first term), the fluid pressure gradient at the bed (second term), and the fluid pressure applied to the topographic gradient (third term). The fourth and fifth group of terms associated with N_R and N_{R_A} are the Newtonian viscous, and the solid-volume-fraction-gradient-enhanced non-Newtonian viscous stresses, respectively. The non-dimensional number N_{R_A} is termed as the mobility number [1]. Finally, the last term is due to the drag force. The term associated with β_s in (2) accounts for the buoyancy-reduced lateral pressure. The solid load is reduced by the buoyancy force by the factor $(1-\gamma)$ as seen in p_{b_s}, Coulomb friction and in the drag term, C_{DG}.

SIMULATION RESULTS AND DISCUSSIONS

Model equations (1)-(2) are written as a set of well-structured, non-linear hyperbolic-parabolic partial differential equations in conservative form with complex source terms. This facilitates numerical integration even when shocks are formed in the field variables [8,11,12]. The model equations are solved in conservative variables $\mathbf{W} = \left(h_s, h_f, m_s, m_f\right)^t$, where $h_s = \alpha_s h$, $h_f = \alpha_f h$ are the solid and fluid contributions to the debris height; and $m_s = \alpha_s h u_s$, $m_f = \alpha_f h u_f$, are the solid and fluid momentum fluxes. The high-resolution shock-capturing Total Variation Diminishing Non-Oscillatory Central (TVD-NOC) scheme is implemented [13-15]. We consider a two-phase subaerial debris flow that hits a fluid dam in the downstream (Fig. 1). The upper part of the channel is inclined ($\zeta = 45°$). The initial triangle is uniformly filled with homogeneous mixture of 50% solid and 50% fluid. The dam consists of 98% fluid and 2% solid grains. The parameter values are: $\phi = 35°$, $\delta = 15°$, $\rho_f = 1,100$ kgm^{-3}, $\rho_s = 2,500$ kgm^{-3}, $N_R = 150,000$, $N_{R_A} = 30$, $Re_p = 1$, $U_T = 1, P = 0.5, J = 1, \chi = 3, \xi = 5, C = 0.5$.

The model analysis includes generation and interactions of debris and fluid waves. The state of the solid volume fraction is essential for the correct prediction of the turbidity currents, sediment transport and deposition in the subaerial and submarine environments. As the two-phase subaerial debris flow hits a fluid dam, a tsunami wave is generated, and a submarine debris wave continues to slide (Fig. 1). The orange and blue colors indicate the volume fractions of the solid and the fluid. At $t = 0$ s, only the solid (orange) is seen while the fluid (blue) is on the back side of the solid. At $t = 2$ s the debris hits the dam to generate a tsunami. The debris mass slides down the slope as a submarine debris flow and the tsunami wave propagates to the right. As the debris continues to hit the dam with higher momentum, the tsunami wave is amplified and more and more fluid mass from the left of the dam is pushed to the right. This results in a hydrodynamic impact vacuum, or crater [16], which increases in time and continues for quite a while. At a further instant ($t = 5$ s), three complex flows occur simultaneously; including (*i*) subaerial debris flow in the upstream region, (*ii*) submarine debris flow in the downstream and in the dam basin, and (*iii*) a super tsunami wave on the surface of the dam. At $t = 5$ s, the submarine debris hits the horizontal basin of the dam and the tsunami becomes a super wave. At $t = 7$ s, it is clearly seen that the submarine debris wave (internal wave) is moving much faster than the free-surface tsunami wave. At $t = 9$ s, the debris mass supply from the upstream is exhausted so that a left-going water wave starts and slowly moves back to the slope side. Then, the height of left side of the tsunami wave is diminished and decreases the hydrodynamic vacuum. Four clearly observable waves exist at this moment; two tsunami waves with one towards the right and another towards the left, and two waves associated with the submarine debris flow, one at the front and another at the tail. A particularly important observation is that, at $t = 9$ s, the submarine debris flow has already hit the distal vertical wall of the dam, but the tsunami is still following it. This time gap may potentially be used to generate an early warning signal. As soon as the debris hits the dam wall ($t = 10$ s), a shock wave of debris material is generated and propagates upstream. At some later time, as the tsunami wave also hits the right wall of the dam and runs-up, the submarine debris shock wave is diffused. After a long time the fluid level in the dam becomes (almost) horizontal (not shown). These behaviors should be an observable natural phenomena, and are simulated here for the first time using a real two-phase flow model with a high resolution shock capturing scheme.

SUMMARY

This paper presents some new aspects of the complex interactions and waves generated from a two-phase debris flow impacting a fluid dam, and how it penetrates the fluid and finally deposits on the bottom of the basin. Simulation results show that for small amount of solid volume fraction in the dam, the submarine debris flow moves substantially faster than the tsunami wave generated by a two-phase debris flow itself. This important result can be used to generate early warning signals in coastal regions, and also to be used to prevent possible catastrophic dam collapses. As the submarine debris flow impinges the distal vertical wall of the dam, a debris shock wave is generated and propagates upstream, which is eventually diffused. The simultaneous dynamic simulation of the two-phase subaerial debris flow, the resulting tsunami generation and propagation upon debris impact at the dam, the subsequent submarine debris flow, and the entire analysis of all three-types of waves and their complex interactions were made possible by applying a new generalized two-phase debris flow model [1]. These results should be observable in nature, and are simulated for the first time with a two-phase mass flow model together with a high resolution shock capturing scheme. This innovative approach allows for the adequate modeling of debris induced tsunami and submarine sediment transport, with applications in hazard mitigation, sedimentology, submarine geodynamics, and the integrity of hydroelectric power plants.

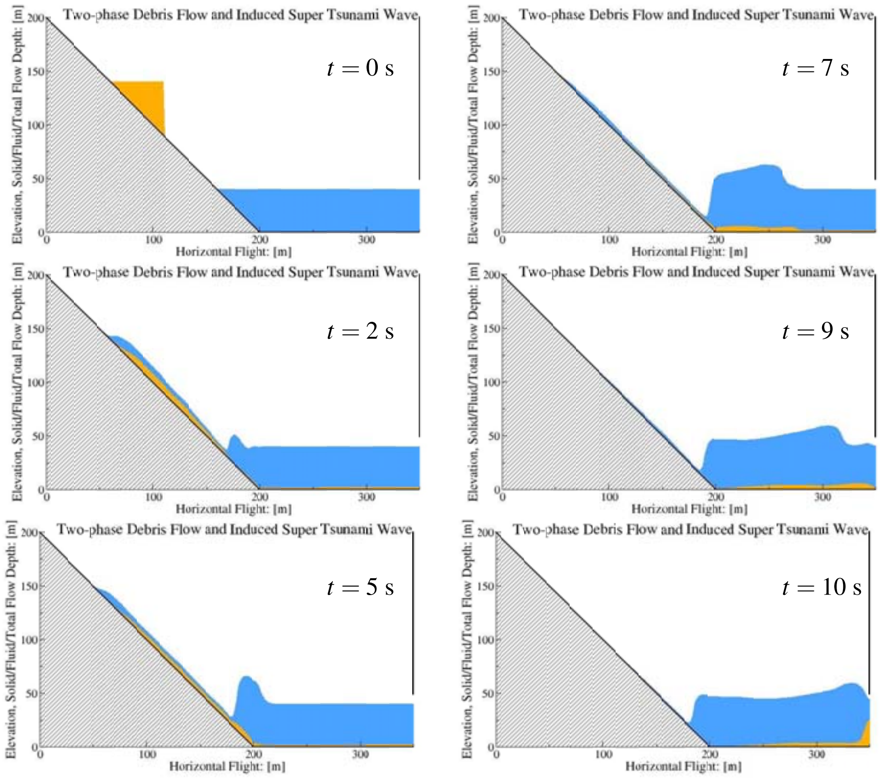

FIGURE 1. Two-phase subaerial debris flow hits a fluid dam ($t = 2$ s), generates tsunami wave, and a submarine debris wave continues to slide down. Orange and blue colors indicate volume fractions of solid and fluid. At $t = 5$ s, tsunami wave is amplified, leading to an increasing hydrodynamic impact vacuum. There are three complex flows taking place simultaneously: subaerial debris flow in the upstream, submarine debris flow in the downstream and at the dam floor, and the surface tsunami wave. At $t = 5$ s, the submarine debris hits the horizontal basin of the dam and the tsunami becomes a super wave. At $t = 7$ s, the submarine debris wave is moving much faster than the tsunami wave. At $t = 9$ s, a left-going water wave starts, and the hydrodynamic vacuum is decreasing. A particularly important observation is: the submarine debris already hits the right wall of the dam but the tsunami is still following the debris mass. This time gap can be used in generating early warning signals. At $t = 10$ s, the submarine debris hits the distal dam wall and a shock wave of debris material is generated that propagates upstream.

REFERENCES

1. S. P. Pudasaini, *J. Geophys. Res.*, doi:10.1029/2011JF002186 (2012).
2. S. Tinti, A. Manucci, G. Pagnoni, A. Armigliato, and F. Zaniboni, *Nat. Hazards Earth Syst. Sci.* **5**, 763-775 (2005).
3. R. Weiss, H. M. Fritz, and K. Wuennemann, *Geophys. Res. Lett.* **36**, L09602, doi: 10.1029/2009GL037814 (2009).
4. S. B. Savage, and K. Hutter, *J. Fluid Mech.* **199**, 177–215 (1989).
5. R. M. Iverson, and R. P. Denlinger, *J. Geophys. Res.* **106**no.B1, 537–552 (2001).
6. S. P. Pudasaini, and K. Hutter, *J. Fluid Mech.* **495**, 193–208 (2003).
7. E. B. Pitman, and L. Le, *Phil. Trans. Royal Society* **A363**, 1573–1602 (2005).
8. S. P. Pudasaini, Y. Wang, and K. Hutter, *Nat. Hazards Earth Syst. Sci.* **5**, 799–819 (2005).
9. T. Takahashi, *Debris Flow: Mechanics, Prediction and Countermeasures*, Taylor & Francis Ltd., 2007.
10. E. D. Fernandez-Nieto, F. Bouchut, D. Bresch, M. J. Castro Diaz, and A. Mangeney, *J. Comput. Phys.* **227**, 7720-7754 (2008).
11. S. P. Pudasaini, *Phys. Fluids* **23**(4), 043301 (2011).
12. S. P. Pudasaini, C. Kröner, *Physical Review E* **78**(4), 041308 (2008).
13. H. Nessyahu, and E. Tadmor, *J. Comput. Phys.* **87**, 408 (1990).
14. Y.-C. Tai, S. Noelle, J. M. N. T. Gray, and K. Hutter, *J. Comput. Phys.* **175**, 269–301 (2002).
15. S. P. Pudasaini, and K. Hutter, *Avalanche Dynamics: Dynamics of Rapid Flows of Dense Granular Avalanches*, Springer Berlin, New York, 2007, pp. 602.
16. F. Mohammed, H. M. Fritz, *Advances in Natural and Technological Hazards Research* **28**, 705-718 (2010).